Producing a new in-situ wind speed product for the Southern Ocean based on acoustic meteorology from biologged southern elephant seals

Anatole Gros-Martial, Gabriel Dubus, Dorian Cazau, Sara Bazin, Christophe Guinet

Producing a New In Situ Wind Speed Product for the Southern Ocean Based on Acoustic Meteorology from Biologged Southern Elephant Seals

ANATOLE GROS-MARTIAL,[a,c,d] GABRIEL DUBUS,[b] DORIAN CAZAU,[c] SARA BAZIN,[d] AND CHRISTOPHE GUINET[a]

[a] *Centre d'Etudes Biologiques de Chizé, CNRS, Villiers-en-Bois, France*
[b] *Sorbonne University, CNRS, Institut d'Alembert UMR 7190, LAM, Paris, France*
[c] *ENSTA, Lab-STICC, UMR CNRS 6285, Brest, France*
[d] *Geo-Ocean, IUEM, Univ. Brest, CNRS, Ifremer, Plouzané, France*

(Manuscript received 17 April 2025, in final form 25 June 2025, accepted 12 August 2025)

ABSTRACT: Obtaining in situ wind speed measurements over the ocean is paramount to (i) better calibrate numerical models and satellite imagery and (ii) increase our understanding of upper ocean processes such as mixed layer depth (MLD) dynamics and air–sea gas exchanges. For instance, increasing wind speeds deepens the MLD through surface turbulence and mixing. In this study, we evaluate the use of acoustic meteorology as an alternative to conventional reanalysis and scatterometer products by training regression models and long short-term memory (LSTM) neural networks on passive acoustic data recorded from biologged elephant seals. The study presents the first LSTM fine-tuned on wind speed data products from the *China–France Oceanography Satellite* (*CFOSAT*) mission, exhibiting remarkably low errors with an average error over all deployments of 0.86 m s^{-1}. Using an innovative validation protocol, by correlating wind speed predictions with collocated MLD measurement, the different models are compared. All models' wind speed predictions exhibit better correlation coefficients with the MLD than the ERA5 reanalysis wind speed products, underscoring the added value of acoustic meteorology in resolving ocean–atmosphere coupling. This work highlights the potential of passive acoustic monitoring as a robust, scalable, and accurate tool for oceanographic and climate studies.

KEYWORDS: Southern Ocean; Wind; Wind gusts; Acoustic measurements/effects; ScatterometerDeep learning

1. Introduction

Ocean winds are critical for improving weather and climate forecasting, supporting marine operations, and advancing environmental monitoring applications. These winds are sampled using both in situ instruments like buoys and ships, and remote sensing tools such as satellite-based microwave radiometers and scatterometers. However, too few buoys are deployed in the Southern Ocean due to the harsh and cold conditions (Venkatesan et al. 2018). The lack of in situ data in such regions is problematic as they are necessary for the calibration of satellites and numerical weather prediction (NWP) and reanalysis models. This is conveyed by important discrepancies in wind measurements, with studies reporting root-mean-square errors (RMSEs) as high as 3.2 m s^{-1} between anemometer and scatterometer data (Derkani et al. 2021). Similarly, Tetzner et al. (2019) highlighted that the ERA5 reanalysis (Hersbach et al. 2023) model in coastal portions of the Southern Antarctic Peninsula underestimated wind speed by 1.48 m s^{-1}.

In addition, most available wind products for the oceans have low temporal resolution. Remote sensing techniques, such as scatterometers for instance, are limited by their orbits, which usually result in repeat cycles longer than 4 days (Bentamy et al. 2021). Reanalysis models, like ERA5 and MERRA-2, for example, provide measurements on a global scale with a temporal resolution of 1 h. However, these models often apply spatial and temporal averaging and do not capture fine temporal-scale wind variability, potentially limiting their accuracy in resolving localized or rapidly evolving events.

Winds in the Southern Ocean are uninterrupted and omnipresent and therefore impact heavily every process at stake in the water column. For instance, they are responsible for the alteration of the sea surface temperature seasonal cycle (Zhang et al. 2024), and their near-endless fetch leads to the generation of rogue waves (Toffoli et al. 2024). Better estimations of wind speed in these regions will help better characterize the mixed layer depth (MLD)—the depth of the upper layer of the ocean with uniform density, quantify the oceanic uptake of CO_2 more accurately, or increase our understanding of sea ice formation (Gregor et al. 2024). Obtaining in situ wind measurements with a fine temporal and spatial scale is therefore paramount to a better qualification of the Southern Ocean sea state and MLD variations. In this study, we investigate the use of acoustic meteorology, defined below, as an alternative and complementary in situ source of fine temporal-scale wind speed estimations in the Southern Ocean.

Knudsen et al. (1948) showed that there is a strong correlation between surface wind speed and underwater ambient noise quantified through the overall pressure level. When wind-generated waves and whitecaps break, they produce a layer of oscillating and cavitating bubbles near the surface. The oscillations of these bubbles are an important noise source, with the intensity of the noise being correlated with the density and height of the bubble layer and therefore with surface wind speed (Franz 1959; Farmer and Vagle 1988; Medwin and Beaky 1989). The development of

Denotes content that is immediately available upon publication as open access.

Corresponding author: Anatole Gros-Martial, grosmartial.anatole@gmail.com

DOI: 10.1175/JTECH-D-25-0037.1

models and algorithms to estimate wind speed from underwater passive acoustic data is thereafter referred to as acoustic meteorology. Many studies have developed such models, starting with regression models including logarithmic laws (Vagle et al. 1990), quadratic laws (Pensieri et al. 2015), or cubic laws (Nystuen et al. 2015). More recently, machine learning models such as random forest classifiers or neural networks, namely, long short-term memory (LSTM) networks, have been evaluated, with the latter giving mean absolute errors (MAEs) as low as 0.84 m s^{-1} (Taylor et al. 2021; Zambra et al. 2022). However, these methods are still being improved, as lower wind speed regimes do not generate waves and therefore produce less sound, and at higher regimes, existing bubbles start absorbing noise from new breaking waves (Vagle et al. 1990; Vakkayil et al. 1996). These limits do not hinder the potential of acoustic meteorology and studies have started addressing these issues, with neural networks able to predict low wind speeds (under 3 m s^{-1}) with an RMSE of 0.84 m s^{-1} and less (Zambra et al. 2022), and with the development of models leveraging low frequencies which successfully estimate wind speed during hurricanes, with results similar to those from aircraft measurements (Wilson and Makris 2008).

Using a multiple linear model, Cazau et al. (2017) have already obtained wind speed estimations from Acousonde acoustic tags deployed on southern elephant seals, obtaining an accuracy of 2 m s^{-1}. Their study shows that depth and diving behavior do not seem to affect the model's performance. Biologging implemented on elephant seals is an excellent way to sample the oceans due to their impressive diving abilities and predictable patterns as well as the long periods they spend at sea. Furthermore, their behavior is independent of the harsh conditions of the Southern Ocean. The data obtained from such deployments have already been of importance in the development of the Marine Mammals Exploring the Oceans Pole to Pole (MEOP)[1] dataset giving access to a new type of oceanographic data in the hard-to-sample polar regions (Roquet et al. 2014; Treasure et al. 2017). In addition, precise wind speed measurements from biologged elephant seals could prove invaluable for the calibration of scatterometers and NWP models, and lead to the creation of new MEOP datasets that include wind speed products collocated with other fine-scale variables such as salinity, temperature, and oxygen.

In this study, we compare different methods for obtaining in situ wind speed data from 12 biologged female elephant seals equipped with acoustic biologgers. We demonstrate the potential of acoustic meteorology for operational deployment by using low-complexity regression models and LSTM neural networks trained on the coarse-grained pseudo-ground-truth wind speed data from the ERA5 reanalysis model. Furthermore, by training the first fine-tuned model on scatterometer data from the *China–France Oceanography Satellite* (*CFOSAT*), we generate a new in situ, high-precision wind speed product for the Southern Ocean, derived from biologged animals. This framework is nested in a long-term vision of embedded codes in the next-generation tags to get real-time in situ wind speed estimations from acoustic data.

[1] https://meop.net/.

2. Data processing

a. Datasets

Between 2017 and 2021, 12 female southern elephant seals were equipped at the end of the breeding season with head-mounted DTAG4 devices (Johnson and Tyack 2003). Three individuals were from the Peninsula Valdés population in Argentina and nine individuals from the Kerguelen population in the Southern Indian Ocean (Fig. 1). The DTAG4s are equipped with a hydrophone sampling at 32 kHz or 38.4 kHz, a pressure sensor and magnetometer sampling at 50 Hz, and an accelerometer sampling at 200 Hz. In addition, a satellite data relayed logger equipped with a CTD sensor (CTD hereafter) from the Sea Mammal Research Unit was deployed on the back of the seal. It logs pressure, temperature, and salinity sampled continuously at 0.5 Hz throughout the deployment.

A reference time frame is constructed for each elephant seal from the first timestamp at which the deployed tag starts logging. This reference time frame has a time step of 3 s to match inertial biologging data processing (section 2). Pressure, temperature, and salinity data are interpolated to match this timeframe. Each available time-referenced data, including acoustic, inertial, depth, and joined wind speed data, for one individual is referred to as a dataset. The overall corpus is therefore composed of 12 such datasets.

Each 3-s time step dataset is then segmented into dives. A dive starts when the elephant seal dives below a depth of 10 m. It consists of the dive itself as well as the following surfacing period up until the animal dives back down under the 10-m threshold.

Data points for which the animal is above a depth of 10 m are then filtered out as a preliminary study showed the first few meters of the water column are not suited for acoustic meteorology. This 10-m threshold matches this study's definition of a dive and the reference depth used for the MLD algorithm (section 3). Dives shorter than 5 min or longer than 40 min are removed from the datasets (see section 2). Table 1 shows the number of dives for each dataset.

1) Passive acoustic data

The overall acoustic data amount to 326 days, 14 h, and 7 min. Recordings are resampled at a sample rate $s_r = 32$ kHz. The passive acoustic data are converted into pressure in Pascals using the instrument's gain, the peak voltage of the analog-to-digital (A–D) converter, and the sensors' sensitivity, which give a total correction factor of 175 dB. The recordings are then cut into 3-s chunks to match the reference datasets. Following the method outlined by Merchant et al. (2015), the power spectral density (PSD) of each chunk is calculated by applying a Hamming window w_n and performing a fast Fourier transform without any overlap on 1024 bin subsignals x. The single-sided power spectrum P_s^x is obtained by squaring the Fourier transform, which is then doubled and normalized:

$$P_{\text{norm}}^x = P_s^x \times 2.0\left[\sum (w_n)^2 \times s_r\right]^{-1}. \quad (1)$$

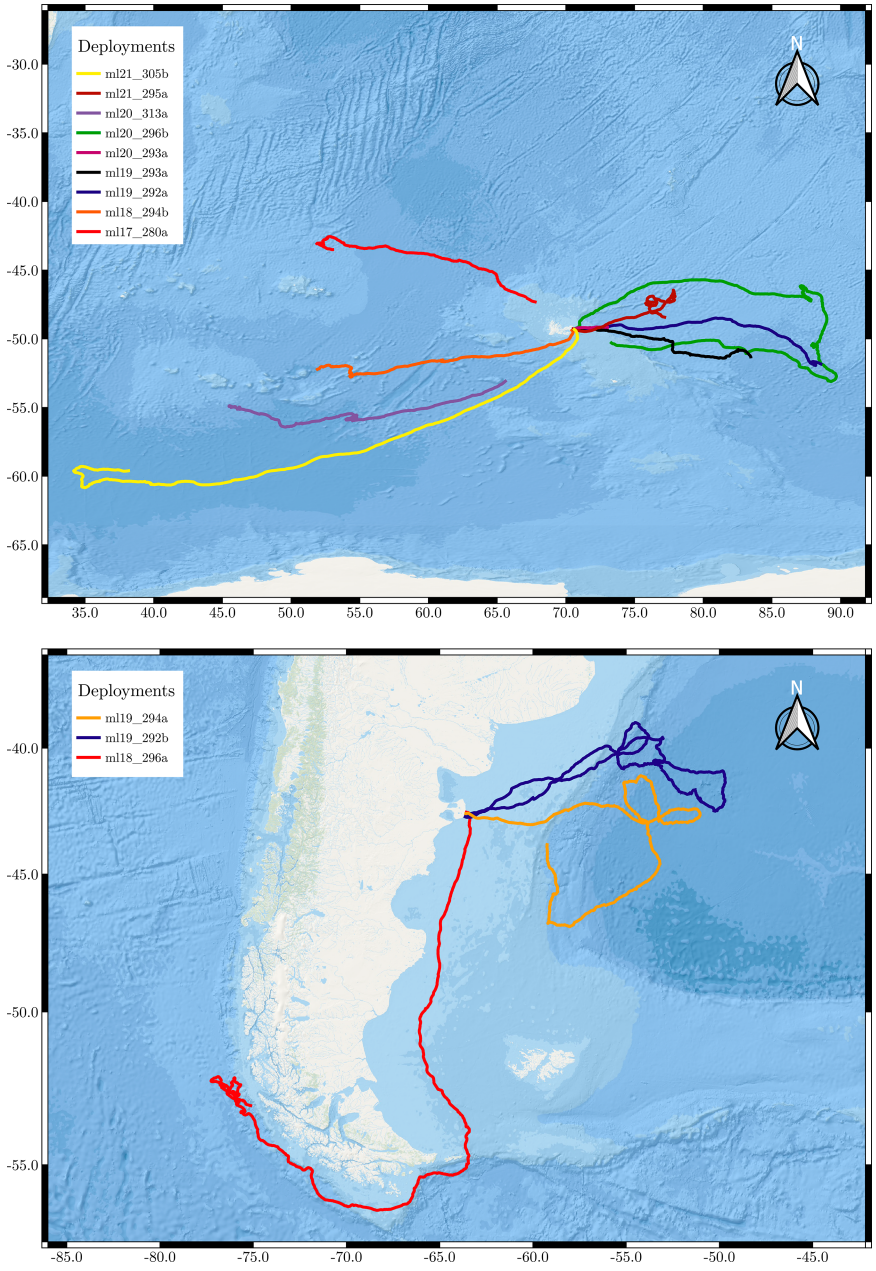

FIG. 1. Trajectories of the 12 female elephant seals with passive acoustic tags. Geographic coverage of the data deployments from the seal population on Kerguelen Island and from the seal population at Peninsula Valdés.

This spectral density is then converted to decibel scale with respect to $p_{\text{ref}} = 1\ \mu\text{Pa}^2\ \text{Hz}^{-1}$:

$$\text{PSD}^x = 10\log\left(\frac{P^x_{\text{norm}}}{p^2_{\text{ref}}}\right). \quad (2)$$

All PSD^x are then averaged to get the final PSD of the 3-s chunk. The final corpus amounts to 14 583 621 PSDs with 513 frequency bins, each having a bandwidth of 31.25 Hz.

2) INERTIAL DATA

Based on the study by Benhamou (2024), the raw accelerometer and magnetometer data are averaged over 3-s windows to get the animal's body posture. The elevation angle (from $-\pi/2$ to $\pi/2$ rad), the bank angle (from $-\pi$ rad to π rad), and the azimuth angle (from $-\pi$ rad to π rad) are computed. Using declination data (Alken et al. 2021) at the last surfacing position, azimuth angles are converted to azimuth with regard to the east. These angles are an indication of the hydrophone's

TABLE 1. Seal datasets and their associated number of dives used in this study. Only the deployments made after year 2018 can be joined to the *CFOSAT* wind speed data (cf. section 2).

Datasets	ml17_280a	ml18_294b	ml18_296a	ml19_292a	ml19_292b	ml19_293a	ml19_294a	ml20_293a	ml20_296b	ml20_313a	ml21_295a	ml21_305b
Number of dives	1847	2339	3296	2059	3772	1987	3599	155	4877	2494	2706	2187
Dives with *CFOSAT*	0	0	0	164	95	133	145	18	129	211	224	101

orientation, animal behavior, and coupled with the depth data, an indication of the animal's speed.

3) MIXED LAYER DEPTH

The MLD was calculated from the potential density anomaly profile σ_0 (with a reference pressure of 0 dbar) derived from the temperature and salinity profiles provided by the CTD tags. For each dive, one MLD value is computed using data sampled during the upward trajectory of the elephant seal. Defining the MLD being arbitrary, the conventions from de Boyer Montégut et al. (2004) were chosen. Using the threshold method on density with a threshold of $\Delta = 0.03$ kg m^{-1} and a reference depth of 10 m, the MLD is found. This method and parameters have already been used successfully in the Southern Ocean (Buongiorno Nardelli et al. 2017).

b. *Meteorological sources*

1) ERA5 REANALYSIS DATA

The ERA5 reanalysis model[2] offers global data on a regular latitude and longitude grid of 0.25° and a temporal resolution of one data point every hour (Hersbach et al. 2023). The model is based on data assimilation by combining the laws of physics with as much observations as possible. Such a data source is particularly useful as it can be joined to every dataset and allows for homogeneous training and validation. What is more, ERA5 reanalysis products accurately estimate the winds in the Southern Ocean, especially temporal variations, showing high correlation with in situ data across all wind speed ranges (Schmidt et al. 2017). In this framework, ERA5 reanalysis u10 and v10 data (10-m eastward neutral wind and 10-m northward neutral wind) are joined to the acoustic dataset using a 3D interpolation to match the elephant's position with a pseudo-ground-truth wind speed value. ERA5 reanalysis wind products have previously been utilized in acoustic meteorology studies (Boittiaux et al. 2020; Zambra et al. 2022), obtaining good results using 10-m neutral wind speed data. In their study, Vagle et al. (1990) showed that the RMSEs for U3, U10, and U10 neutral wind speed were of 0.56, 0.63, and 0.59 m s^{-1}, respectively, with a similar correlation coefficient of 0.97 with wind data from a buoy. As a result, no conversion to surface wind speed was applied. Similarly, other studies, including those introducing the models discussed in section 1, also rely on 10-m wind speed data (Zedel et al. 1999; Reeder et al. 2011; Pensieri et al. 2015; Hildebrand et al. 2021). Figure 2 shows the distributions of the PSDs as a function of ERA5 reanalysis wind speed for each dataset.

2) *CFOSAT*

The *CFOSAT* scatterometer provides a precise source of local wind speed data, making it well suited for serving as ground truth for acoustic meteorology. For wind speeds over the oceans, the RMSE between *CFOSAT* measurements and

[2] https://cds.climate.copernicus.eu/datasets/reanalysis-era5-single-levels?tab=overview.

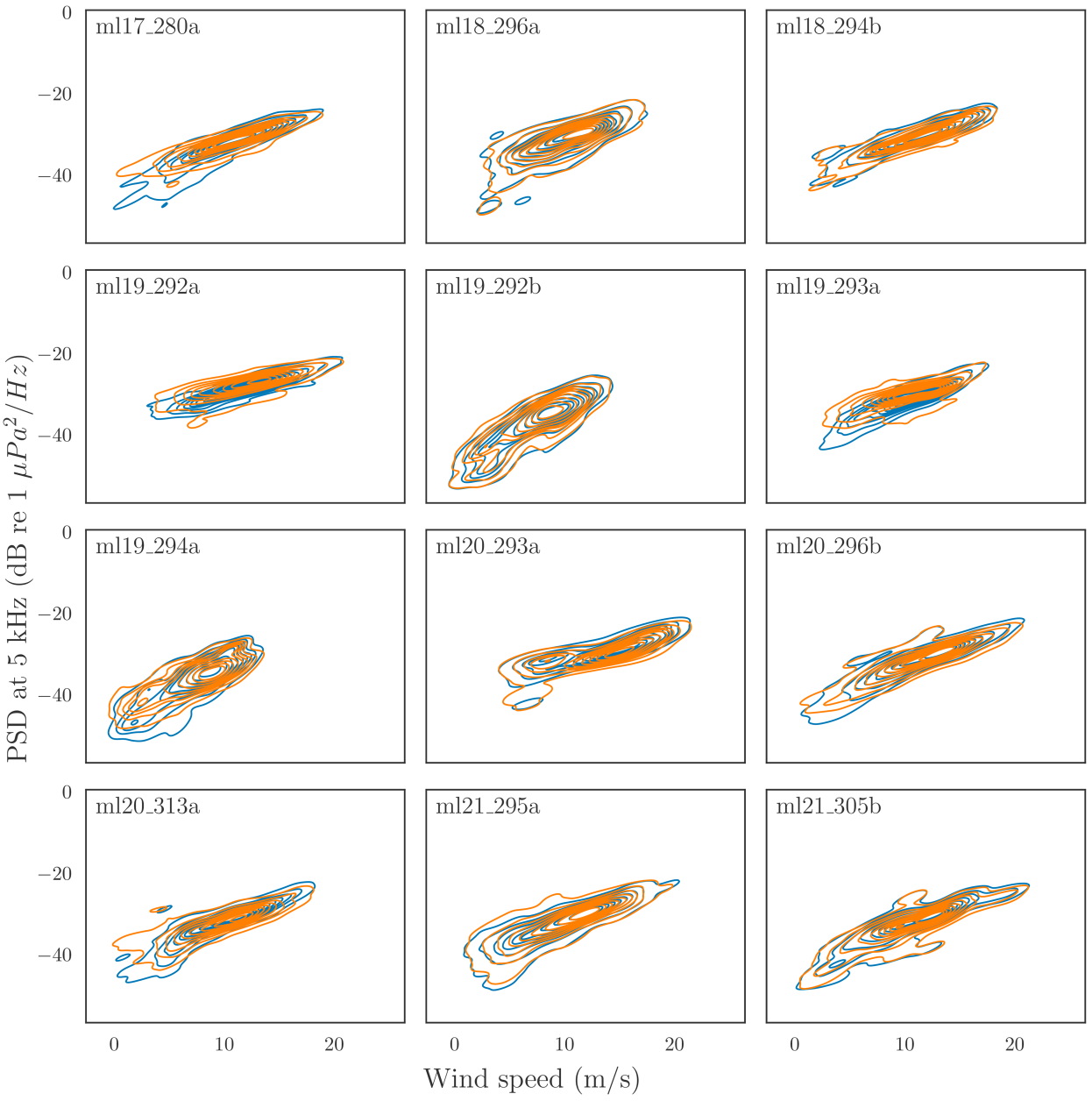

FIG. 2. PSDs at 5 kHz as a function of the corresponding wind speed from the ERA5 reanalysis model for all 12 individuals. Orange density curves are for downward trajectories, and blue density curves are from upward trajectories. The bottom phases of dives are ignored.

buoy observations is 1.39 m s^{-1}, making it a relevant source of data for model training (Ye et al. 2021). However, due to the limited temporal resolution—as the satellite has a repeat cycle of a couple of days—the ground truth volume is insufficient for initial model training. Furthermore, as the satellite was launched in 2018, only the deployments from 2019 to 2021 are useful here. However, *CFOSAT* wind data remains an ideal source for fine-tuning models that have initially been trained with ERA5 reanalysis data. Scatterometer data were thus retained for fine-tuning whenever two or more observation beams were available, regardless of the measured wind speed range. Figure 3 compares the two pseudo-ground-truth data together, namely, ERA5 reanalysis and *CFOSAT*. The RMSE between the two sources is 1.08 m s^{-1}. Although most measurements are similar, the disparity increases for lower wind speeds (under 10 m s^{-1}).

While other satellite wind products are available, the *CFOSAT* was selected for fine-tuning as it has not been assimilated into the ERA5 reanalysis model—unlike ASCAT or SEAWINDS for instance—providing an independent data source for additional training. Moreover, since the study was funded by CNES, preference was given to using data from their satellite, *CFOSAT*.

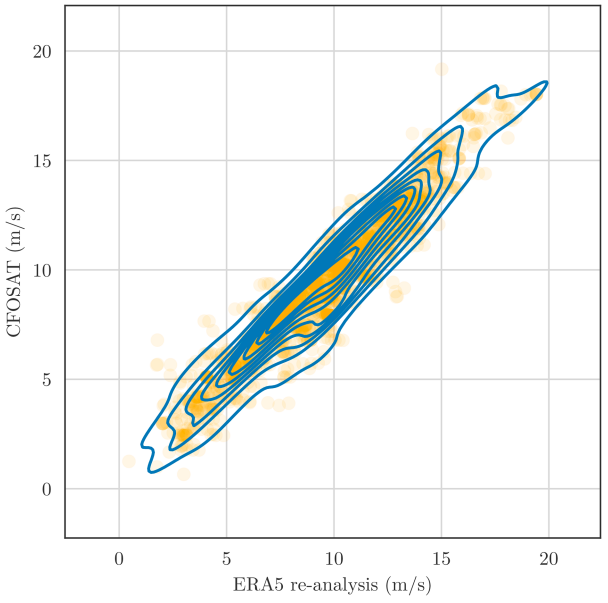

FIG. 3. Comparison of *CFOSAT* and ERA5 reanalysis wind speed data. Each orange point represents the wind speed for both sources at the time and locations of a surfacing individual. Transparency is used for better visualization of data density. Contour lines represent the areas with similar densities. The dives used for this analysis are summarized in Table 1.

c. *Model selection and training routine*

Multiple regression models have been developed to estimate wind speed from underwater passive acoustic recordings. A benchmark of five such models was evaluated using a reference dataset corpus (Gros-Martial et al. 2025). In this study, two models are applied: a logarithmic model, which is the most widely used in the literature (Piggott 1964; Shaw et al. 1978; Evans et al. 1984; Vagle et al. 1990; Chapman and Cornish 1993; Ma and Nystuen 2005; Nystuen et al. 2015; Hildebrand et al. 2021), and a two-regime linear-quadratic model already evaluated on SES data (Pensieri et al. 2015; Cazau et al. 2017). In recent years, deep learning models have been successfully trained on underwater passive acoustic data to estimate surface wind speed. This trend is specific not only to acoustic meteorology but also to physical oceanography as a whole, with both fields rapidly evolving and benefiting from the development of computational resources and data collection techniques (Sonnewald et al. 2021). Machine learning approaches are now used for a wide range of tasks with applications in data assimilation—such as estimating errors or improving observation interpolation—ocean modeling—such as forecasting or detecting climate events—and ocean observation—such as improving ocean sampling or classifying eddies, for instance (Bauchot et al. 2025). Given that wind regimes exhibit temporal patterns, models capable of temporal learning, like recurrent neural networks (RNNs) and LSTMs, should be preferred. Since LSTM models have been previously applied with promising results (Zambra et al. 2022; Trucco et al. 2022, 2023), this study also adopts an LSTM approach.

To apply a model to the acoustic data of a specific individual, the training process for all models is similar. Table 1 shows the amount of training data for each deployment. The corpus is divided into 11 elephant seals for training and one for validation. Each individual is used once as the validation set, following a cross-validation protocol. In a real-time wind measurement scenario, data can only be transmitted while the elephant is surfacing; therefore, the aim of the study is to make one wind speed prediction per dive. The target label is either the pseudo-ground-truth data from ERA5 reanalysis or *CFOSAT* averaged during the considered dive. The overall corpus of datasets offers a remarkable experimental setup to assess and improve model generalization capability across different years, locations, wind distributions, bathymetry, soundscapes, distances to shore, and swimming behaviors of the elephants.

1) REGRESSION MODELS

Two regression laws put forth by Pensieri et al. (2015) and Hildebrand et al. (2021) are used as reference. Models are trained using wind data U in meters per second corresponding to the 10-m wind speed, as provided by the ERA5 reanalysis dataset. For each model, three experiments are carried out using the cross-validation protocol. As the regression models can only take one input per dive, the frequency and temporal dimensions of the PSDs need to be pooled. When elephant seals go out to sea after fasting during the breeding season, they are denser than water and have different swimming behaviors when diving down or swimming back up to the surface. For the first experiment, model training uses the mean PSD during the entirety of the dive, the second experiment estimates wind speed from the PSDs averaged during the downward trajectories where the animal has little swimming activity and glides down, and in the final experiment, models are trained only using the PSDs averaged over the upward trajectories where the animal swims actively. For the first experiment, different frequencies are tested, with $f \in \{50, 100, 200, 300, 500, 1000, 2500, 5000, 8000, 10\,000, 12\,000, 15\,000, 16\,000\}$ Hz. The best frequency is then used for the two other experiments.

The first model is a two-regime linear-quadratic model proposed by Pensieri et al. (2015) [Eqs. (3) and (4)],

$$U = a_1 \times \mathrm{PSD}_f - b_1, \tag{3}$$

$$U = a_2 \times \mathrm{PSD}_f^2 + b_2 \times \mathrm{PSD}_f + c_2, \tag{4}$$

with a_1 and b_1 for Eq. (3) and a_2, b_2, and c_2 for Eq. (4) being trainable parameters for each corpus split. The regime shift between Eqs. (3) and (4) occurs at a wind speed of 5.5 m s^{-1} with Eqs. (3) and (4) being used for low and high wind speeds, respectively.

The second model, inspired from Hildebrand et al. (2021), is based on a logarithmic relationship between noise power and wind speed:

$$\mathrm{PSD}_f = a + 20 \times b \times \log_{10}(U) - 10 \times c \times \log_{10}(f), \tag{5}$$

where a, b, and c are trainable parameters and f is the frequency at which the noise power is computed.

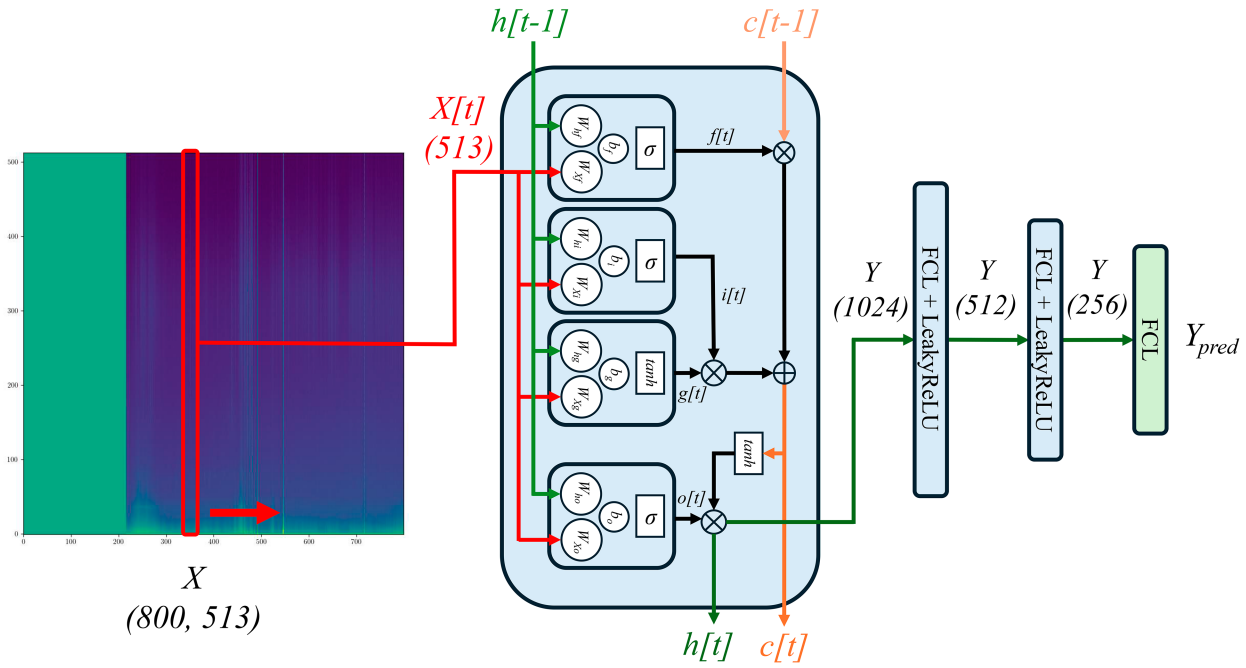

FIG. 4. Schema of the LSTM model. Each dive is formatted into a padded input of size (800 513) [or size (800 517) if inertial and depth data are added], which is fed sequentially into a LSTM cell. The final hidden state of size 1024 is passed through two FCLs with LeakyReLU activations to produce the final wind speed estimation per dive. During fine-tuning on *CFOSAT* data, the blue blocks indicate the components with frozen weights and biases, while the green block (final FCL) is the only trainable layer. For visualization purposes, the red rectangle representing $X[t]$ was drawn wider, although only one temporal bin is fed to the LSTM.

2) NEURAL NETWORK

LSTM neural networks (Hochreiter and Schmidhuber 1997) are renowned for their adequate applications for time series prediction tasks. They can also handle high-dimensional inputs; therefore, all available frequencies and timestamps during a dive are considered, and dives are no longer segmented and averaged for downward trajectory or upward trajectory. Acoustic data are cropped between −90 and 40 dB re 1 μPa^2 Hz^{-1} to limit the impact of outliers during the normalization process. All input data are normalized using a max–min rescaling before being fed to the LSTM. For training purposes, each input is zero-padded to a maximum sequence length of 800 or 40 min, to feed batches of 64 samples to the model. Dives longer than 40 min were removed as too much padding could be detrimental in the training process. Two experiments are considered: One training is based solely on the acoustic data (513 frequency bins or features), and the other has depth and the inertial angles as input as well (517 features). Each of the input data has for the target value the average wind speed during the dive. The chosen model comprises a single recurrent unit with a hidden layer size of 1024 features. The LSTM layer is followed by three fully connected layers (FCLs), reducing the input size to 512 and to 256 before resulting in the final output. The Adam optimizer is used with a learning rate of 0.0001 and a weight decay of 0.0001. The loss function is the mean square error loss. The training protocol for the regression models is kept, with 11 datasets making up the training set, and the final dataset being used as validation. For each of the 12 runs, the model with the lowest loss computed on the validation set after 30 epochs is saved.

3) FINE-TUNING ON *CFOSAT* DATA

To obtain better prediction, scatterometer data from *CFOSAT* are used to fine-tune each of the 12 models. Weights and biases from the previous trainings, with inertial and depth data added to the inputs and ERA5 reanalysis data as the target, are loaded. The recurrent unit and the first two FCLs are frozen, and the weights and biases of the last FCL are updated by training on dives with available *CFOSAT* data as a new target wind speed (Fig. 4). As mentioned previously, performance can only be obtained for tags deployed after 2018. However, predictions can still be obtained for each dataset of the corpus as training data from the *CFOSAT* are available for each split. This fine-tuned LSTM model will be referred to as FT LSTM.

4) VALIDATING MODELS USING THE MIXED LAYER DEPTH

When models are trained on pseudo-ground-truth data, a significant challenge arises in the validation process. ERA5 reanalysis and *CFOSAT* products both exhibit inaccuracies and discrepancies, particularly in regions such as the Southern Ocean. Additionally, as model training and validation are not consistently based on labels from a single data source, direct performance comparisons become difficult. Therefore, an independent data source is necessary for robust model validation. Several studies have demonstrated a direct relationship

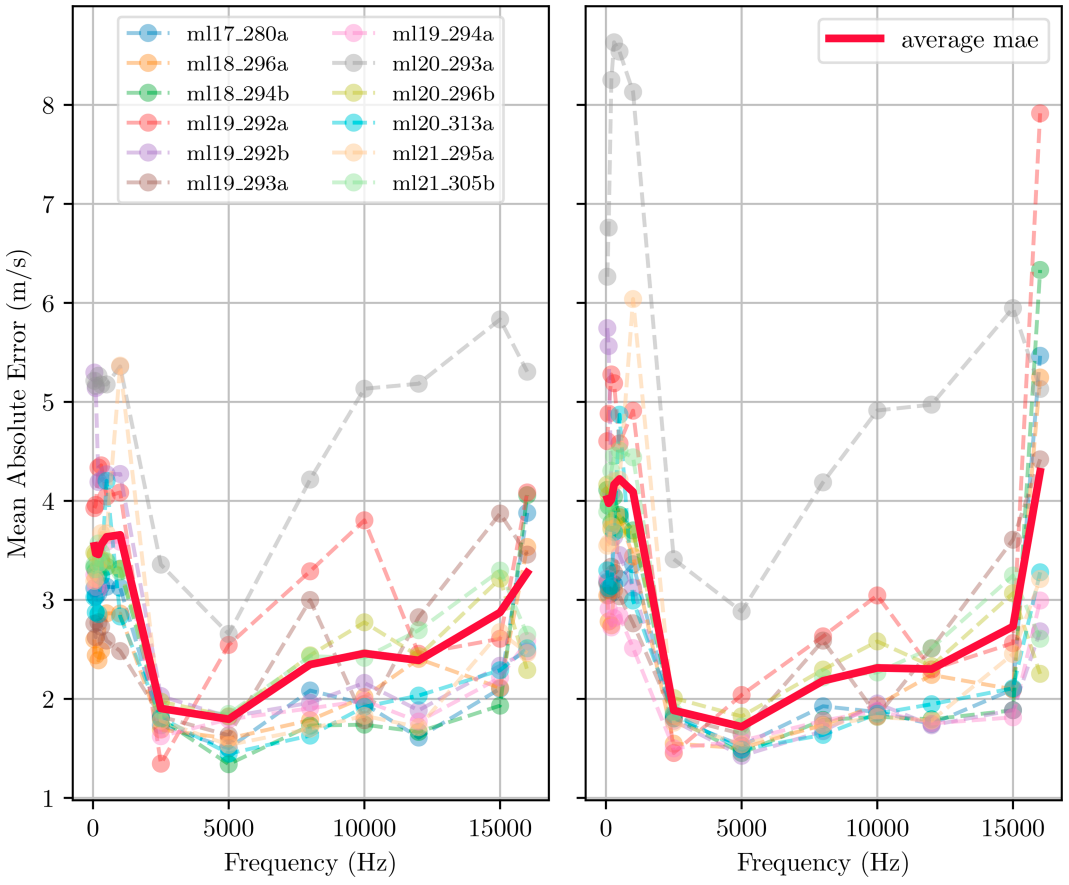

FIG. 5. MAE between estimation from the (left) two-regime linear-quadratic model and (right) logarithmic model and ERA5 reanalysis wind speed data for 13 frequencies (at 50, 100, 200, 300, 500, 1000, 2500, 5000, 8000, 10 000, 12 000, 15 000, and 16 000 Hz).

between MLD and surface wind speed, with wind forcing increasing the MLD (Pollard et al. 1973; Kitaigorodskii et al. 1979; Price et al. 1986; Álvarez et al. 2016; Ushijima and Yoshikawa 2020; Wang et al. 2024). As outlined in section 3, temperature and salinity data give MLD measurements collocated with wind speed estimates. Correlating wind speed predictions from acoustic meteorology models with these MLD values derived from CTD profiles can thus provide an indication of model relevance.

3. Models' performance

a. *Best frequency for wind estimation*

In the first experiment, models are trained using the average PSD from each dive to compare the performance of the logarithmic and two-regime linear-quadratic models across different frequencies. The results are shown in Fig. 5, highlighting which frequency is best suited for acoustic meteorology under the conditions of this study involving biologged southern elephant seals with DTAG4s. For both models, the best frequency for wind estimation is around 5 kHz, which is therefore chosen to train the regression models for the rest of the study. Lower frequencies, under 2500 Hz, show important errors, with a marked drop off in performance. The MAE increases steadily for frequencies higher than 5 kHz, reaching errors similar to low frequencies for the 16-kHz frequency.

b. *Model trained on ERA5 pseudo ground truth*

Once the frequency for regression models was fixed at 5 kHz, different segments of the dives, with different swimming behaviors from the elephant seals, were used for wind speed estimations. The regression models trained on the upward trajectories of the elephant seals have the best predictions (Table 2) with the two-regime linear-quadratic and logarithmic models having MAEs of 1.30 and 1.41 m s^{-1}, respectively (Fig. 6). The models trained on the downward trajectories still predict ERA5 reanalysis pseudo ground truth, though with less precision, having a MAE

TABLE 2. RMSE (m s^{-1}) of estimated wind speed for the three experiments using the logarithmic and two-regime models at 5000 Hz.

	Logarithmic	Two-regime
Upward	1.86	1.66
Downward	2.17	1.89
Dive	2.01	1.75

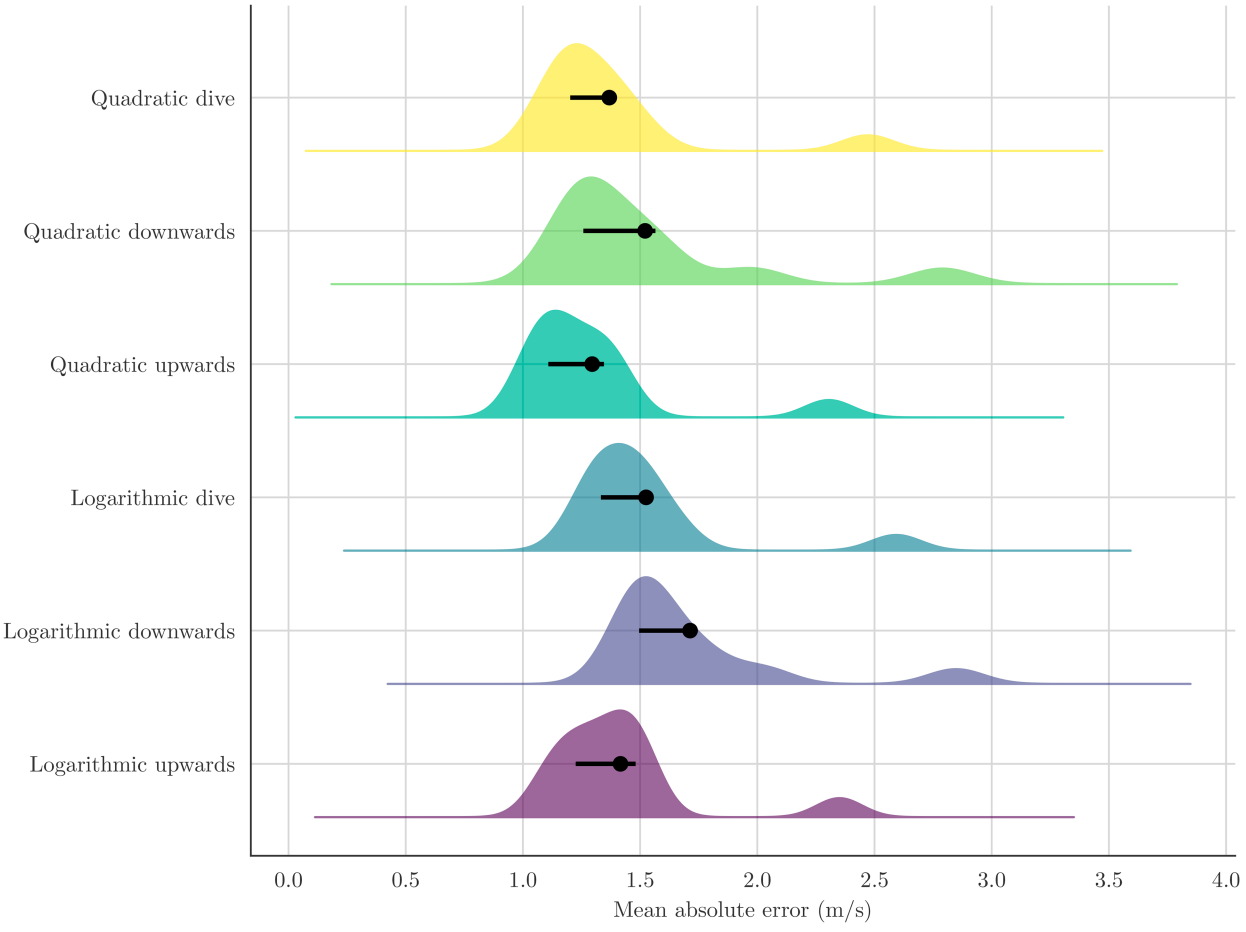

FIG. 6. MAE densities for the regression models across the 12 datasets. The first and third quantiles are represented by the horizontal bar. The average MAE for each model is indicated by the central marker.

of 1.52 m s^{-1} for the two-regime model and of 1.71 m s^{-1} for the logarithmic model. Finally, models trained on the PSDs averaged throughout the entirety of each dive perform marginally worse than those trained on the upward trajectories, with MAE values of 1.37 and 1.53 m s^{-1}. Therefore, the regression models trained on upward trajectories are chosen as reference and hereafter referred to as the two-regime and logarithmic models. Finally, for all evaluation experiments on these distinct dive segments, the logarithmic model has higher errors than the two-regime linear-quadratic model, with the RMSE being between 0.20 and 0.28 m s^{-1} higher. This observed error variability is similar to the improvements gained from selecting specific trajectory segments, as the best logarithmic model and the worst two-regime model have similar RMSEs of 1.86 and 1.89 m s^{-1}, respectively.

Following the evaluation of both regression models across various frequencies and dive segments, identifying the two-regime model fitted at 5 kHz on upward trajectories as the best model, the study next examines the relevance of a deep learning approach to the task. As shown in Fig. 7 and Table 3, neural network models outperform the two-regime model, and other regression models, in predicting ERA5 reanalysis pseudo ground truth, with an error of 1.15 m s^{-1} for the LSTM trained using only the acoustic features. This corresponds to a MAE decrease of 0.15 m s^{-1} with regard to the two-regime model. However, the standard deviation of the residuals is similar between the two models, increasing from 1.52 to 1.58 m s^{-1} for the LSTM and the two-regime model, respectively (Table 4). Furthermore, Fig. 7 illustrates that the LSTM does not consistently outperform the two-regime model across all wind speed ranges; however, the two-regime model exhibits higher MAEs near the regime transition and tends to underestimate high wind speeds (starting from 10 m s^{-1}).

A closer examination of the different neural network results reveals that the LSTM models, with and without the inertial and depth data as input, perform similarly. The LSTM with inertial and depth data shows a slight improvement in predictive performance of 0.02 m s^{-1} (Table 3). Validation accuracies per dataset show important discrepancies with MAE varying from 0.91 to 1.38 m s^{-1}. For the rest of the study, only the model with added inertial and depth data will be considered and referred to as LSTM.

c. *Fine-tuning on satellite data*

Table 3 presents the results for the FT LSTM, assessing the added value of incorporating *CFOSAT* data into the training scheme and whether fine-tuning on scatterometer data yields

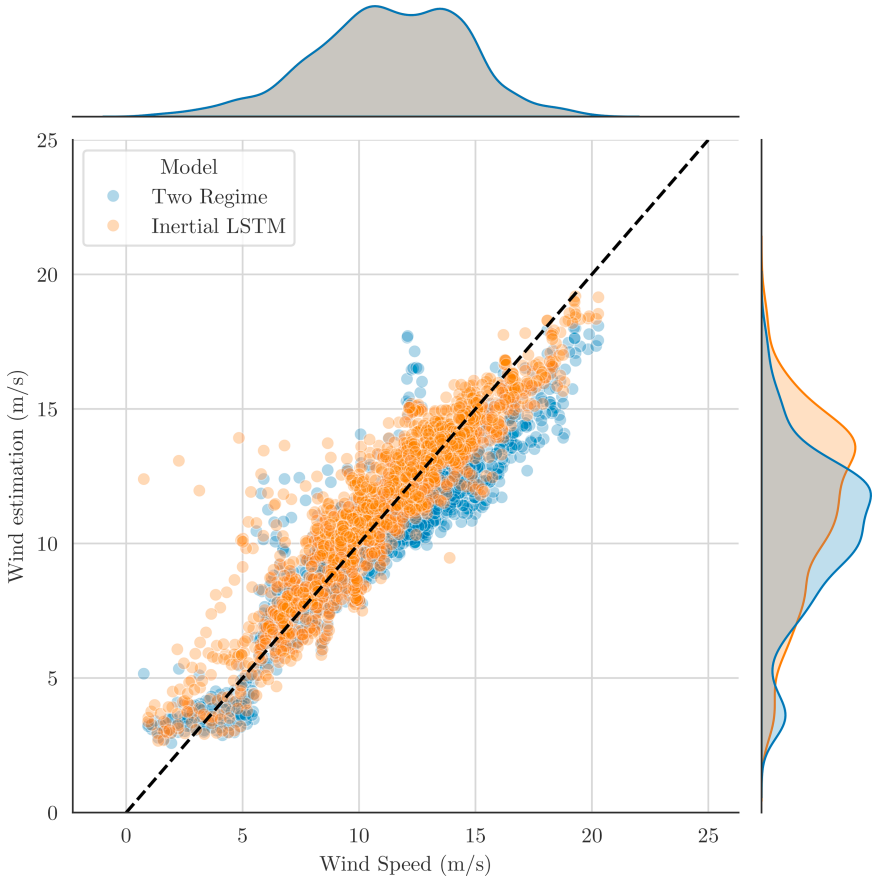

FIG. 7. LSTM model and two-regime model estimations vs pseudo-ground-truth wind speed from ERA5 reanalysis.

better results. The FT LSTM, validated using *CFOSAT* data, shows a significant improvement in accuracy, with an average MAE of 0.86 m s^{-1}, which represents a 0.27 m s^{-1} decrease in error from the LSTM results. The lowest error across all datasets is of 0.64 m s^{-1}. When validated against the ERA5 reanalysis wind speed pseudo ground truth, the FT LSTM still performs well with an absolute deviation of 1.20 m s^{-1} (Table 3).

d. Model validation

With models trained and evaluated on two different products, being ERA5 reanalysis and *CFOSAT* wind speed,

TABLE 3. MAE (m s^{-1}) for the two neural networks. From left to right, the columns show the results for the LSTM model validated on ERA5 reanalysis data, the LSTM trained with inertial data validated on ERA5 reanalysis data, the FT LSTM model validated on all *CFOSAT* data, and the FT LSTM model validated on all ERA5 reanalysis data, respectively.

	LSTM	Inertial LSTM	FT LSTM on *CFOSAT*	FT LSTM on ERA5
ml17_280a	0.92	0.91		0.99
ml18_296a	1.38	1.38		1.48
ml18_294b	1.00	0.99		1.02
ml19_292a	1.18	1.14	0.74	1.22
ml19_292b	1.27	1.23	0.85	1.29
ml19_293a	0.93	0.93	0.78	1.24
ml19_294a	1.36	1.29	1.09	1.37
ml20_293a	1.32	1.28	0.94	1.18
ml20_296b	1.03	1.05	0.64	1.08
ml20_313a	0.96	0.95	0.75	0.98
ml21_295a	1.21	1.24	1.16	1.29
ml21_305b	1.19	1.19	0.80	1.21
Average	1.15	1.13	0.86	1.20

TABLE 4. Standard deviation error (m s^{-1}) between the two-regime model, LSTM and FT LSTM estimations, and ERA5 reanalysis wind speed.

	Two-regime	LSTM	FT LSTM
ml17_280a	1.30	1.22	1.21
ml18_294a	1.64	1.96	1.84
ml18_294b	1.33	1.35	1.33
ml19_292a	1.66	1.40	1.62
ml19_292b	1.57	1.65	1.68
ml19_293a	1.33	1.25	1.20
ml19_294a	1.50	1.69	1.68
ml20_293a	2.18	1.54	1.71
ml20_296b	1.51	1.45	1.44
ml20_313a	1.28	1.50	1.45
ml21_295a	2.03	1.60	1.57
ml21_305b	1.59	1.65	1.61
Average	1.58	1.52	1.53

models are further evaluated by relating the estimated wind speed with in situ colocalized MLD values. Figure 8 illustrates how these wind estimations from different models correlate to the MLD across various temporal lags. All models follow a similar trend, with their relationship gradually strengthening over time and the correlation coefficient peaking for the MLD at t_0 + 14 h. The pseudo-ground-truth ERA5 reaches its peak slightly later, at t_0 + 15 h. All acoustic meteorology models show similar correlation values with a peak correlation between 0.318 and 0.342. Among all models, the LSTM consistently shows the strongest relationship. In contrast, the ERA5 reanalysis wind speed exhibits the weakest correlation with the MLD across all temporal lags.

To better visualize the wind speed estimations from the different models, Fig. 9 represents a time series of the ERA5 reanalysis and *CFOSAT* wind speed data and three models (two-regime, LSTM, and FT LSTM). All three acoustic meteorology models exhibit fine temporal-scale variations not present in the ERA5 reanalysis data. This variability is also present in the few *CFOSAT* wind speed measurements available. Furthermore, while all wind products vary similarly, extreme wind events and low wind speeds show the highest discrepancies between estimations from the three acoustic meteorology models and the ERA5 wind speed. On 5 November, both neural networks predict a wind gust, whereas the ERA5 model predicts wind speeds under 5 m s^{-1}.

Table 4 shows the standard deviation of the residuals of each model when evaluated against ERA5 reanalysis wind speed. While the results per dataset vary, the average std across all datasets is very similar for the three models with

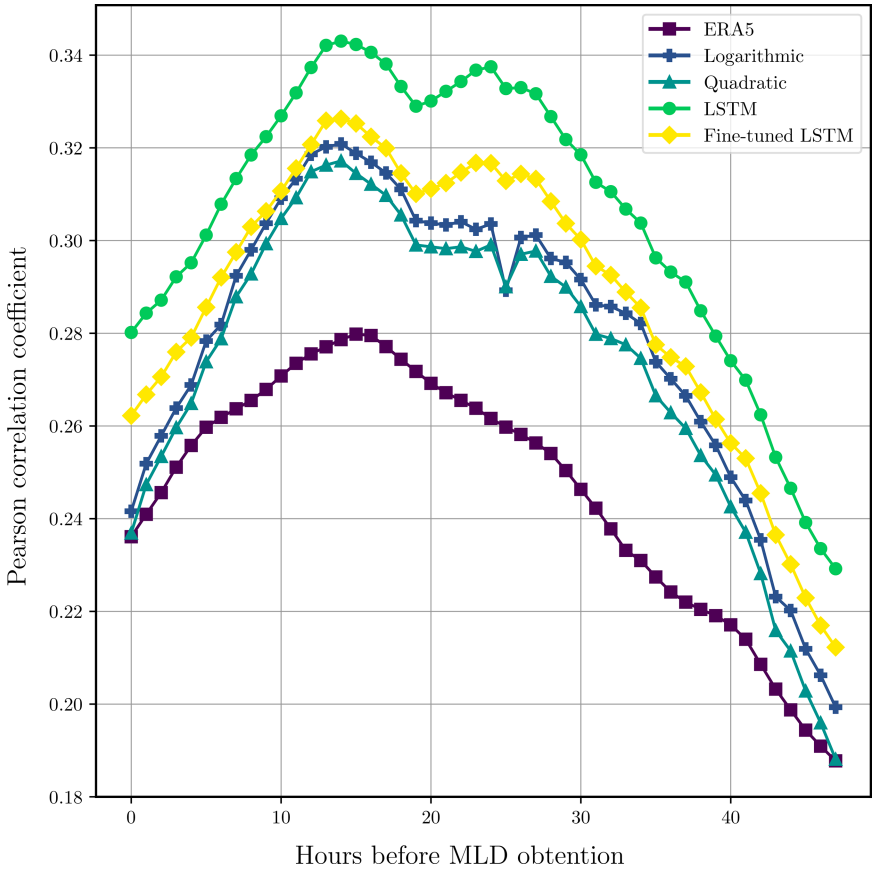

FIG. 8. Correlation between MLD and wind speed estimations for all elephant seals, as a function of temporal lag (h).

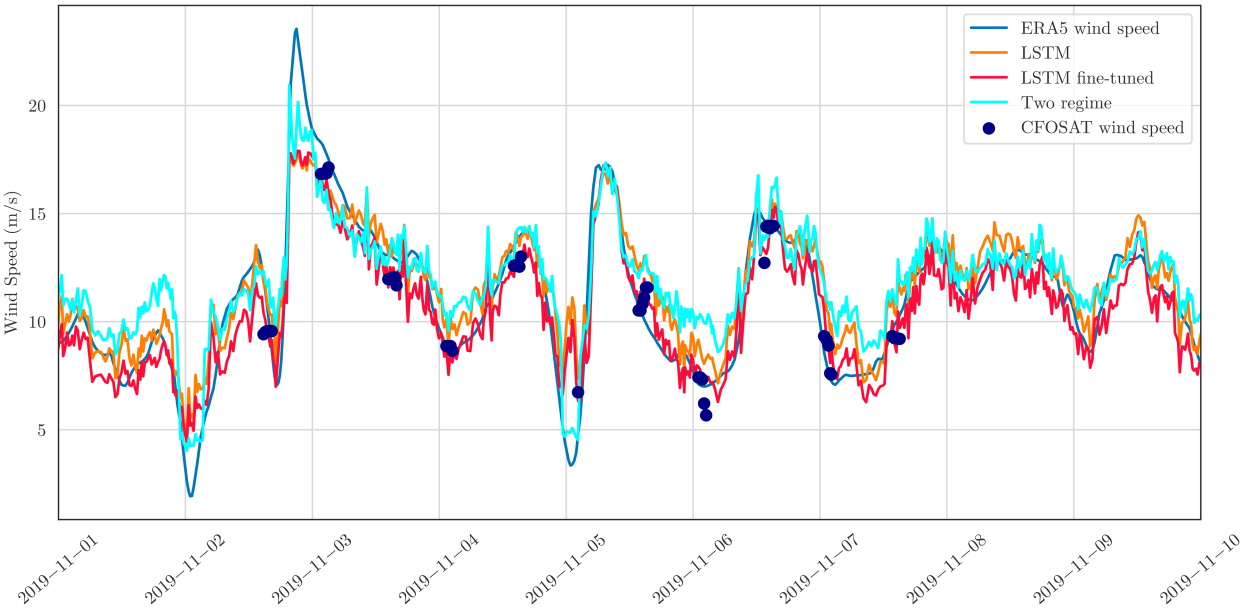

FIG. 9. Example of predictions from three models (two-regime, inertial LSTM, and FT LSTM) over 9 days. Pseudo-ground-truth wind speed data from ERA5 reanalysis (solid line) and *CFOSAT* (scatter points) are also plotted.

standard deviations of 1.58, 1.52, and 1.53 m s^{-1} for the two-regime model, LSTM, and FT LSTM, respectively. Figure 9 corroborates this result, as all three acoustic models capture both the fine-scale temporal variations and the broader temporal trends from the ERA5 reanalysis wind product.

4. Discussion

a. *Best regression model*

With the deployments from the present study differing in both time and space, (i) wind distributions are different for each dataset, (ii) the bathymetry and shore distance change for each individual, and (iii) each elephant seal has its own swimming behavior; therefore, individual models are expected to be different. However, the final models obtained by training on 11 elephant seal datasets are robust and generalize well to new individuals. As elephant seals leave their colony after breeding and fasting, elephant seal females are in poor body conditions and have less body fat. As a consequence, they are negatively buoyant (i.e., denser than seawater) and they remain so during most of their postbreeding foraging trip (Richard et al. 2014). Consequently, when diving downward, they can glide with little to no swimming effort (Aoki et al. 2011; Richard et al. 2014). In contrast, when ascending toward the surface, they need to actively stroke. Acoustic data from these upward trajectories reveal that flow noise is a significant sound source. However, the results show that regression models calibrated using data from upward trajectories outperformed those from downward trajectories. There could be two main reasons for this. First, the wind noise models were deliberately calibrated using a higher frequency (5 kHz) outside the range dominated by flow noise, where wind-generated noise is expected to be the primary contributor. Second, the hydrophone on DTAG4s is positioned at the front of the tag. While the hydrophones are omnidirectional, the tag itself blocks noise originating from behind the animal. When the seal swims toward the surface, the tag is oriented toward the sound source of interest, increasing the likelihood of detecting noise from breaking waves and whitecaps. Furthermore, while higher frequencies are also outside of the range contaminated by flow noise and are more likely dominated by wind-generated noise, attenuation makes them less relevant for analysis especially with increasing depth (Vagle et al. 1990), making 5 kHz the ideal frequency for wind speed estimation from biologged elephant seals. This value is consistent with published regression models and studies reporting optimal frequencies for wind speed estimation between 2 and 6 kHz, with good results up to 10 kHz (Lemon et al. 1984; Zedel et al. 1999; Pensieri et al. 2015; Hildebrand et al. 2021).

Moreover, the two-regime model consistently outperformed the logarithmic model. This discrepancy likely stems from the behavior of the logarithmic models for high PSD values at 5 kHz. Some of these PSD values are outliers, meaning dives with high acoustic intensity at low wind speeds, and heavily impact the regression models. Such outliers could be due to the animal's behavior or the presence of other sound sources, though rare, such as precipitation, odontocete vocalizations, or shipping traffic, which generate noise at 5 kHz. Furthermore, the two-regime model, by fitting five parameters rather than the three of the logarithmic model, is better able to fit the data. However, both regression models outperform the existing models for wind speed estimation using biologged elephant seals, with Cazau et al. (2017) reporting RMSE between model estimations and a derived ASCAT wind speed ranging from 1.9 to 2.1 m s^{-1} for drift phases and from 2.6 to 3.4 m s^{-1} for active swimming phases (Table 2). Note that

different hydrophones were used in their study, with Acousonde tags being deployed on the back of the animal.

b. Added value of neural networks

The LSTM outperforms published regression models, thanks to the higher number of features in input data, but also because of the complexity of the model and number of parameters that are fitted. At wind speeds below 3 m s^{-1}, minimal surface noise is generated, leading to the models' inability to accurately estimate these conditions. The neural network leverages richer input data—incorporating multiple frequencies and temporal features—to better identify and estimate these lower wind speeds. Furthermore, the regression models are particularly impacted by outliers, namely, sound recordings containing other noise sources than wind-generated noise. This susceptibility results in the erroneous estimation of wind events exceeding 20 m s^{-1} and a general underestimation of surface wind speeds when additional noise sources raise the mean PSD, skewing predictions. These events should be flagged beforehand when using a regression model (Vagle et al. 1990; Nystuen and Selsor 1997). Based on Fig. 6, with regression models trained on upward trajectories—i.e., positive elevation angle—having lower MAE than for the downward trajectories—i.e., negative elevation angle, the addition of inertial data to models was supposed to be significant. However, results show that adding inertial features in the LSTM model only improves performance slightly. The model's performance increases only by 0.02 m s^{-1} because inertial data are implicitly encoded in the temporal component of the LSTM, with the first temporal bins of the input corresponding to the downward trajectories and the last to the upward trajectories. The small improvement can be linked to a better estimation of wind speed during drift dives, where the animal has no swimming activity, and therefore, less flow noise is present in the recordings (Richard et al. 2014). Similarly, regression models could be adapted to take depth into account (Hildebrand et al. 2021). While depth had little impact on LSTM performance, similar to the effect of adding inertial data, adapting the wind model for a specific depth or incorporating depth as a parameter could help refine the prediction.

Neural networks are computationally expensive during training and remain heavy and complex models especially for onboard deployments. Models of intermediate complexity, tree-based models—such as random forests or gradient boosting—kernel-based models—such as SVMs—or regularized linear models—such as LASSO (least absolute shrinkage and selection operator) or ridge—could have been tested. However, past studies have focused on fitting regression models to the acoustic and wind speed data, and more recently on LSTM architectures (Nystuen et al. 2015; Pensieri et al. 2015; Hildebrand et al. 2021; Trucco et al. 2022; Zambra et al. 2022). Although some random forest algorithms have previously been applied (Taylor et al. 2021), only the low-complexity regression models and the LSTM approach were chosen in this study to illustrate both the baseline performance of easily deployable models and the best accuracy achievable with state-of-the-art methods on biologged elephant seal data.

c. Fine-tuning on CFOSAT

Fine-tuning on *CFOSAT* data was expected to improve the LSTM model's performance, the main reason being that the temporal and spatial scale of *CFOSAT* data is more closely aligned with those of our study case compared to ERA5 reanalysis. With a coarse resolution of 1 h and on a grid of 0.25° (or a longitudinal distance of 18 km at a latitude of −49°), ERA5 reanalysis provides smoothed wind speed products at large spatial and temporal scales. For a hydrophone at depth h in meters, 90% of the signal is composed of sources coming from a surface listening area $\mathcal{A}_{90\%}$ of size $\mathcal{A}_{90\%} = \pi(3h)^2$ (Ma and Nystuen 2005). This represents an area of 10.18 km^2 at a depth of 600 m, and only 1.13 km^2 at a depth of 200 m for seal acoustic data. The scale of the hydrophone's integration area is about 40 times finer than the ERA5 reanalysis spatial resolution. With dives lasting about 20 min, the temporal resolution of our models is also about three times finer than ERA5 reanalysis. While *CFOSAT* products have a similar spatial resolution to ERA5, their much higher temporal resolution allows for training on co-occurring wind speeds. Although these differences in spatial and temporal resolution, as well as in the integration area and spatial averaging, inevitably introduce uncertainties into the acoustic meteorology models, these datasets remain essential for training in remote regions where no in situ observations are available.

The results of the FT LSTM are comparable to studies training LSTMs using collocated anemometers with a fixed mooring. Such studies report MAEs ranging from 0.62 to 0.76 m s^{-1} (Trucco et al. 2022) or of 0.665 m s^{-1} for a K-cross-validation protocol (Trucco et al. 2023). Using an autoencoder on the same dataset (Pensieri et al. 2015) yields an RMSE between 0.89 and 0.97 m s^{-1} (Zambra et al. 2022). The consistently low MAE scores observed across all FT LSTM models indicate that training on scatterometer data yields highly accurate wind speed estimations, outperforming those obtained using the ERA5 reanalysis dataset. Similarly to acoustic meteorology—which estimates wind characteristics based on the acoustic signatures generated by bubble formation from wind-driven surface waves—scatterometers infer wind speed by analyzing the backscatter signal produced by surface roughness and wind-induced oceanic ripples. Both methods are fundamentally grounded in the physical interactions between wind and the sea surface. In contrast, reanalysis models synthesize data from diverse observational sources and employ numerical models to interpolate spatial and temporal gaps.

The results show that the LSTM model trained on ERA5 reanalysis data exhibits a stronger correlation with the MLD compared to the FT LSTM model, while the pseudo-ground-truth ERA5 wind speed data shows the weakest correlation (Fig. 8). These differences likely arise from the complex nature of the mixed layer, which deepens under sustained wind forcing over large spatial and temporal scales—better captured by the LSTM trained on smoothed data from ERA5 reanalysis than the FT LSTM, thereby resulting in a higher Pearson correlation. However, the MLD is also highly sensitive to short-term wind variability and gust events, which are not well-represented in

the coarser-resolution ERA5 reanalysis data (Fig. 9). This limitation likely accounts for the lower correlation observed with the ERA5 wind speed measurements. Furthermore, most studies use the 0.03 kg m^{-1} threshold to compute the MLD average data over specific time periods and areas—typically over a day and on a grid of 0.5°–1°—to analyze long-term variations and regional differences. However, the MLD fluctuations in this study's context are driven by local wind variations that occur on finer spatial and temporal scales. Further research on the best density threshold for this context might help refine the validation protocol.

d. *Acoustic as an alternate source of wind speed*

Figure 9 highlights how ERA5 reanalysis data are smoothed out compared to acoustic meteorology products. These fine temporal-scale variations are due to the variations in the surrounding soundscape from (i) changes in wind speed and in wind-generated noise and (ii) other sound sources likely due to the elephant seals' movements. Elephant seals typically forage in areas with little to no human activity. Other sound sources in these regions, including baleen whale vocalizations, seismic activity, and breaking ice caps, are low-frequency sounds and are not picked up by the 5-kHz frequency. These long-ranging and extended sources are not possible explanations for small temporal-scale variations seen in Fig. 9. Potential sound sources that could interfere with the 5-kHz frequency—such as rainfall or vocalizations from odontocetes (clicks, whistles, or buzzes)—are expected to be minimal or negligible with regard to the duration of the study period. The regression models however could be heavily influenced by transient noise from the elephant seal's movement, which accounts for some of the variation. However, both the LSTM and FT LSTM, by leveraging multiple frequencies and timestamps, are able to filter out these outliers. This is further evidence that acoustic meteorology picks up on fine temporal-scale wind speed variations (Cazau et al. 2017).

While acoustic meteorology has been explored and developed over the years, its full potential and relevance in ocean–atmosphere studies are still being evaluated. This study presents a compelling case for its application, through regression models and neural networks, providing an accurate wind speed product capable of capturing fine-scale wind variations as well as low and high wind speed events. Notably, FT LSTM models trained on scatterometer data had exceptionally low MAE values, highlighting the ability of acoustic meteorology models to give precise in situ wind speed measurements and this through a simple neural network architecture. Moreover, integrating acoustic meteorology with floats or moored hydrophones presents opportunities for long-term monitoring of air–sea interactions. In particular, improving the in situ wind speed products could enhance estimates of CO_2 uptake, which is tightly linked to surface turbulence and MLD variability. However, these benefits depend critically on the recording strategy. Continuous acoustic recordings, as used in this study, preserve the high temporal resolution necessary for resolving short-term wind dynamics. In contrast, hydrophones operating on duty cycles or those triggered by depth (e.g., on mobile platforms) risk losing this precision, potentially limiting their utility for fine-scale ocean–atmospheric coupling studies.

5. Conclusions

This study highlights the relevance of acoustic meteorology in obtaining fine temporal-scale in situ wind speed products. The results show that neural network approaches, here a LSTM, significantly outperform traditional regression models due to their ability to leverage richer input data and handle noise more effectively. This study also presents, to the best of our knowledge, the first model fine-tuned on satellite scatterometer data, significantly increasing the accuracy of the predictions. Given the limited size of the *CFOSAT* dataset, the results show that opportunistic training on scatterometer data, ship-based wind speed measurements, or other alternative sources can greatly benefit acoustic meteorology. Finally, this study underscores the potential of acoustic meteorology as an alternative wind speed measurement method. The strong correlation between mixed layer depth variations and wind-generated noise supports the use of acoustic meteorology models as an in situ ground truth wind speed product. Unlike ERA5 reanalysis data, which is constrained by its hourly resolution, acoustic recordings capture very localized short-term wind variations, making them particularly valuable for studying oceanographic processes.

Acknowledgments. All *CFOSAT* data are provided by courtesy of CNSA and CNES (under science proposals 4583 & 4916.) (Liu et al. 2020). The authors would like to thank the French Polar Institute (IPEV) for their logistic and financial support of the program, as well as all the staff who contributed to the data collection in the field. We would also like to thank the CNRS for their funding of the Eléphants de Mer Sentinelles de l'Océan Austral (Elephant Seals as Southern Ocean Sentinels) through the SNO-MEMO observatory and the SEE-Life Elephant de mer observatory. Finally, the authors extend their thanks and gratitude to the CNES for funding this research and for their financial support of the program.

Data availability statement. Wind data are freely available using the ECMWF API for ERA5 reanalysis data (https://doi.org/10.24381/cds.adbb2d47) and through AVISO + CNES for *CFOSAT* data (https://aviso-data-center.cnes.fr/user/ssalto/modules/1861). CTD data are available on the MEOP database (https://meop.net/). Acoustic and inertial data are available upon reasonable request by contacting the authors. All codes used in this study are found in GitHub (https://github.com/gmanatole/Biologging_Toolkit.git).

REFERENCES

Alken, P., and Coauthors, 2021: International Geomagnetic Reference Field: The thirteenth generation. *Earth Planets Space*, **73**, 49, https://doi.org/10.1186/s40623-020-01288-x.

Álvarez, E., J. Zanella, A. Pescio, and W. Dragani, 2016: An estimation of the effect of a possible wind speed increase on the

ocean mixed layer depth at the northern Patagonian continental shelf. *Reg. Stud. Mar. Sci.*, **6**, 87–95, https://doi.org/10.1016/j.rsma.2016.03.004.

Aoki, K., and Coauthors, 2011: Northern elephant seals adjust gliding and stroking patterns with changes in buoyancy: Validation of at-sea metrics of body density. *J. Exp. Biol.*, **214**, 2973–2987, https://doi.org/10.1242/jeb.055137.

Bauchot, P., A. Drémeau, F. Sévellec, and R. Fablet, 2025: Neural data assimilation for regime shift monitoring of an idealized AMOC chaotic model. *J. Adv. Model. Earth Syst.*, **17**, e2024MS004462, https://doi.org/10.1029/2024ms004462.

Benhamou, S., 2024: Of heading, posture and body rotations derived from data acquired by animal-borne accelerometers, magnetometers and gyrometers, kernel density estimation of the corresponding spherical distributions, and fine-scale movement reconstruction. arXiv, 2310.05820v9, https://doi.org/10.48550/arXiv.2310.05820.

Bentamy, A., S. A. Grodsky, G. Cambon, P. Tandeo, X. Capet, C. Roy, S. Herbette, and A. Grouazel, 2021: Twenty-seven years of scatterometer surface wind analysis over eastern boundary up-welling systems. *Remote Sens.*, **13**, 940, https://doi.org/10.3390/rs13050940.

Boittiaux, C., P. Duc, N. Longépé, S. Pensieri, R. Bozzano, and D. Cazau, 2020: Multi-modal deep learning models for ocean wind speed estimation. *2020 MACLEAN: Machine Learning for Earth Observation Workshop,* Virtual, 1–6, https://ceur-ws.org/Vol-2766/paper5.pdf.

Buongiorno Nardelli, B., S. Guinehut, N. Verbrugge, Y. Cotroneo, E. Zambianchi, and D. Iudicone, 2017: Southern ocean mixed-layer seasonal and interannual variations from combined satellite and in situ data. *J. Geophys. Res. Oceans*, **122**, 10 042–10 060, https://doi.org/10.1002/2017JC013314.

Cazau, D., J. Bonnel, J. Jouma'a, Y. L. Bras, and C. Guinet, 2017: Measuring the marine soundscape of the Indian Ocean with southern elephant seals used as acoustic gliders of opportunity. *J. Atmos. Oceanic Technol.*, **34**, 207–223, https://doi.org/10.1175/JTECH-D-16-0124.1.

Chapman, N. R., and J. W. Cornish, 1993: Wind dependence of deep ocean ambient noise at low frequencies. *J. Acoust. Soc. Amer.*, **93**, 782–789, https://doi.org/10.1121/1.405440.

de Boyer Montégut, C., G. Madec, A. S. Fischer, A. Lazar, and D. Iudicone, 2004: Mixed layer depth over the global ocean: An examination of profile data and a profile-based climatology. *J. Geophys. Res.*, **109**, C12003, https://doi.org/10.1029/2004JC002378.

Derkani, M. H., and Coauthors, 2021: Wind, waves, and surface currents in the Southern Ocean: Observations from the Antarctic circumnavigation expedition. *Earth Syst. Sci. Data*, **13**, 1189–1209, https://doi.org/10.5194/essd-13-1189-2021.

Evans, D. L., D. R. Watts, D. Halpern, and S. Bourassa, 1984: Oceanic winds measured from the seafloor. *J. Geophys. Res.*, **89**, 3457–3461, https://doi.org/10.1029/JC089iC03p03457.

Farmer, D. M., and S. Vagle, 1988: On the determination of breaking surface wave distributions using ambient sound. *J. Geophys. Res.*, **93**, 3591–3600, https://doi.org/10.1029/JC093iC04p03591.

Franz, G. J., 1959: Splashes as sources of sound in liquids. *J. Acoust. Soc. Amer.*, **31**, 1080–1096, https://doi.org/10.1121/1.1907831.

Gregor, L., J. Shutler, and N. Gruber, 2024: High-resolution variability of the ocean carbon sink. *Global Biogeochem. Cycles*, **38**, e2024GB008127, https://doi.org/10.1029/2024GB008127.

Gros-Martial, A., and Coauthors, 2025: Benchmarking models for ocean wind speed estimation based on passive acoustic monitoring. *OCEANS 2025 Brest*, Brest, France, Institute of Electrical and Electronics Engineers, 1–10, https://ieeexplore.ieee.org/document/11104747.

Hersbach, H., and Coauthors, 2023: ERA5 hourly data on single levels from 1940 to present. Copernicus Climate Change Service (C3S) Climate Data Store (CDS), accessed 1 February 2023, https://doi.org/10.24381/cds.adbb2d47.

Hildebrand, J. A., K. E. Frasier, S. Baumann-Pickering, and S. M. Wiggins, 2021: An empirical model for wind-generated ocean noise. *J. Acoust. Soc. Amer.*, **149**, 4516–4533, https://doi.org/10.1121/10.0005430.

Hochreiter, S., and J. Schmidhuber, 1997: Long short-term memory. *Neural Comput.*, **9**, 1735–1780, https://doi.org/10.1162/neco.1997.9.8.1735.

Johnson, M., and P. Tyack, 2003: A digital acoustic recording tag for measuring the response of wild marine mammals to sound. *IEEE J. Oceanic Eng.*, **28**, 3–12, https://doi.org/10.1109/JOE.2002.808212.

Kitaigorodskii, S., J. C. Nihoul, and A. Loffet, 1979: Review of the theories of wind-mixed layer deepening. *Elsevier Oceanogr. Ser.*, **25**, 1–33, https://doi.org/10.1016/S0422-9894(08)71119-X.

Knudsen, V., O. R. Alford, and J. Emling, 1948: Underwater ambient noise. *J. Mar. Res.*, **7**, 410–429, https://doi.org/10.5772/intechopen.93057.

Lemon, D. D., D. M. Farmer, and D. R. Watts, 1984: Acoustic measurements of wind speed and precipitation over a continental shelf. *J. Geophys. Res.*, **89**, 3462–3472, https://doi.org/10.1029/JC089iC03p03462.

Liu, J., and Coauthors, 2020: First results from the rotating fan beam scatterometer onboard CFOSAT. *IEEE Trans. Geosci. Remote Sens.*, **58**, 8793–8806, https://doi.org/10.1109/TGRS.2020.2990708.

Ma, B. B., and J. A. Nystuen, 2005: Passive acoustic detection and measurement of rainfall at sea. *J. Atmos. Oceanic Technol.*, **22**, 1225–1248, https://doi.org/10.1175/JTECH1773.1.

Medwin, H., and M. M. Beaky, 1989: Bubble sources of the Knudsen Sea noise spectra. *J. Acoust. Soc. Amer.*, **86**, 1124–1130, https://doi.org/10.1121/1.398104.

Merchant, N. D., K. M. Fristrup, M. P. Johnson, P. L. Tyack, M. J. Witt, P. Blondel, and S. E. Parks, 2015: Measuring acoustic habitats. *Methods Ecol. Evol.*, **6**, 257–265, https://doi.org/10.1111/2041-210X.12330.

Nystuen, J. A., and H. D. Selsor, 1997: Weather classification using passive acoustic drifters. *J. Atmos. Oceanic Technol.*, **14**, 656–666, https://doi.org/10.1175/1520-0426(1997)014<0656:WCUPAD>2.0.CO;2.

——, M. N. Anagnostou, E. N. Anagnostou, and A. Papadopoulos, 2015: Monitoring Greek seas using passive underwater acoustics. *J. Atmos. Oceanic Technol.*, **32**, 334–349, https://doi.org/10.1175/JTECH-D-13-00264.1.

Pensieri, S., R. Bozzano, J. A. Nystuen, E. N. Anagnostou, M. N. Anagnostou, and R. Bechini, 2015: Underwater acoustic measurements to estimate wind and rainfall in the Mediterranean Sea. *Adv. Meteor.*, **2015**, 612512, https://doi.org/10.1155/2015/612512.

Piggott, C. L., 1964: Ambient sea noise at low frequencies in shallow water of the Scotian Shelf. *J. Acoust. Soc. Amer.*, **36**, 2152–2163, https://doi.org/10.1121/1.1919337.

Pollard, R. T., P. B. Rhines, and R. O. R. Y. Thompson, 1973: The deepening of the wind-mixed layer. *Geophys. Fluid Dyn.*, **4**, 381–404, https://doi.org/10.1080/03091927208236105.

Price, J. F., R. A. Weller, and R. Pinkel, 1986: Diurnal cycling: Observations and models of the upper ocean response to

diurnal heating, cooling, and wind mixing. *J. Geophys. Res.*, **91**, 8411–8427, https://doi.org/10.1029/JC091iC07p08411.

Reeder, D. B., E. S. Sheffield, and S. M. Mach, 2011: Wind-generated ambient noise in a topographically isolated basin: A pre-industrial era proxy. *J. Acoust. Soc. Amer.*, **129**, 64–73, https://doi.org/10.1121/1.3514379.

Richard, G., J. Vacquié-Garcia, J. Jouma'a, B. Picard, A. Génin, J. P. Y. Arnould, F. Bailleul, and C. Guinet, 2014: Variation in body condition during the post-moult foraging trip of Southern elephant seals and its consequences on diving behaviour. *J. Exp. Biol.*, **217**, 2609–2619, https://doi.org/10.1242/jeb.088542.

Roquet, F., and Coauthors, 2014: A Southern Indian Ocean database of hydrographic profiles obtained with instrumented elephant seals. *Sci. Data*, **1**, 140028, https://doi.org/10.1038/sdata.2014.28.

Schmidt, K. M., S. Swart, C. Reason, and S.-A. Nicholson, 2017: Evaluation of satellite and reanalysis wind products with in situ wave glider wind observations in the Southern Ocean. *J. Atmos. Oceanic Technol.*, **34**, 2551–2568, https://doi.org/10.1175/JTECH-D-17-0079.1.

Shaw, P. T., D. R. Watts, and H. T. Rossby, 1978: On the estimation of oceanic wind speed and stress from ambient noise measurements. *Deep-Sea Res.*, **25**, 1225–1233, https://doi.org/10.1016/0146-6291(78)90015-2.

Sonnewald, M., R. Lguensat, D. C. Jones, P. D. Dueben, J. Brajard, and V. Balaji, 2021: Bridging observations, theory and numerical simulation of the ocean using machine learning. *Environ. Res. Lett.*, **16**, 073008, https://doi.org/10.1088/1748-9326/ac0eb0.

Taylor, W. O., M. N. Anagnostou, D. Cerrai, and E. N. Anagnostou, 2021: Machine learning methods to approximate rainfall and wind from acoustic underwater measurements (February 2020). *IEEE Trans. Geosci. Remote Sens.*, **59**, 2810–2821, https://doi.org/10.1109/TGRS.2020.3007557.

Tetzner, D., E. Thomas, and C. Allen, 2019: A validation of ERA5 reanalysis data in the southern Antarctic Peninsula—Ellsworth land region, and its implications for ice core studies. *Geosciences*, **9**, 289, https://doi.org/10.3390/geosciences9070289.

Toffoli, A., and Coauthors, 2024: Observations of Rogue Seas in the Southern Ocean. *Phys. Rev. Lett.*, **132**, 154101, https://doi.org/10.1103/PhysRevLett.132.154101.

Treasure, A., and Coauthors, 2017: Marine mammals exploring the oceans pole to pole: A review of the MEOP consortium. *Oceanography*, **30** (2), 132–138, https://doi.org/10.5670/oceanog.2017.234.

Trucco, A., A. Barla, R. Bozzano, E. Fava, S. Pensieri, A. Verri, and D. Solarna, 2022: Compounding approaches for wind prediction from underwater noise by supervised learning. *IEEE J. Oceanic Eng.*, **47**, 1172–1187, https://doi.org/10.1109/JOE.2022.3162689.

——, ——, ——, S. Pensieri, A. Verri, and D. Solarna, 2023: Introducing temporal correlation in rainfall and wind prediction from underwater noise. *IEEE J. Oceanic Eng.*, **48**, 349–364, https://doi.org/10.1109/JOE.2022.3223406.

Ushijima, Y., and Y. Yoshikawa, 2020: Mixed layer deepening due to wind-induced shear-driven turbulence and scaling of the deepening rate in the stratified ocean. *Ocean Dyn.*, **70**, 505–512, https://doi.org/10.1007/s10236-020-01344-w.

Vagle, S., W. G. Large, and D. M. Farmer, 1990: An evaluation of the WOTAN technique of inferring oceanic winds from underwater ambient sound. *J. Atmos. Oceanic Technol.*, **7**, 576–595, https://doi.org/10.1175/1520-0426(1990)007<0576:AEOTWT>2.0.CO;2.

Vakkayil, R., H. Graber, and W. Large, 1996: Oceanic winds estimated from underwater ambient noise observations in SWADE. *OCEANS 96: MTS/IEEE Conf. Proc.: The Coastal Ocean–Prospects for the 21st Century*, Fort Lauderdale, FL, Institute of Electrical and Electronics Engineers, 45–51, https://doi.org/10.1109/OCEANS.1996.572450.

Venkatesan, R., K. Ramesh, A. Kishor, N. Vedachalam, and M. A. Atmanand, 2018: Best practices for the ocean moored observatories. *Front. Mar. Sci.*, **5**, 469, https://doi.org/10.3389/fmars.2018.00469.

Wang, Y., and Coauthors, 2024: Enhanced wind mixing and deepened mixed layer in the Pacific Arctic shelf seas with low summer sea ice. *Nat. Commun.*, **15**, 10389, https://doi.org/10.1038/s41467-024-54733-w.

Wilson, J. D., and N. C. Makris, 2008: Quantifying hurricane destructive power, wind speed, and air-sea material exchange with natural undersea sound. *Geophys. Res. Lett.*, **35**, L10603, https://doi.org/10.1029/2008GL033200.

Ye, H., and Coauthors, 2021: Evaluation of CFOSAT scatterometer wind data in global oceans. *Remote Sens.*, **13**, 1926, https://doi.org/10.3390/rs13101926.

Zambra, M., D. Cazau, N. Farrugia, A. Gensse, S. Pensieri, R. Bozzano, and R. Fablet, 2022: Learning-based estimation of in-situ wind speed from underwater acoustics. arXiv, 2208.08912v1, https://doi.org/10.48550/arXiv.2208.08912.

Zedel, L., L. Gordon, and S. Østerhus, 1999: Ocean ambient sound instrument system: Acoustic estimation of wind speed and direction from a subsurface package. *J. Atmos. Oceanic Technol.*, **16**, 1118–1126, https://doi.org/10.1175/1520-0426(1999)016⟨1118:OASISA⟩2.0.CO;2.

Zhang, Y., C. Chen, S. Hu, G. Wang, K. McMonigal, and S. M. Larson, 2024: Summer westerly wind intensification weakens Southern Ocean seasonal cycle under global warming. *Geophys. Res. Lett.*, **51**, e2024GL109715, https://doi.org/10.1029/2024GL109715.